Power-Frequency Characteristics of the TRAPATT Diode Mode of High Efficiency Power Generation in Germanium and Silicon Avalanche Diodes

By D. L. SCHARFETTER

(Manuscript received October 23, 1969)

We calculate in this paper the output power obtainable, versus frequency, for TRAPATT diodes. This high efficiency mode of operation is analyzed by means of a simplified model for both germanium and silicon avalanche diodes. The model evolved from a study of detailed computer simulations of experimental diode-circuit systems. The simplified analysis assumes: (i) The avalanche zone transit, plus the recovery time to the swept-out state, occurs in a half period of the TRAPATT frequency. (ii) The ratio of IMPATT frequency to TRAPATT frequency is 3:1. (iii) The diode area is chosen to provide 10 ohms negative resistance, a reasonable value for microwave circuits. The calculated electrical characteristics agree well with experimental observations. Consideration of circuit and thermal limitations results in a design for maximum power output for a millimeter wave silicon oscillator. Power output in excess of 1 watt CW, with an efficiency of 40 percent, is predicted at a frequency of 50 GHz.

I. INTRODUCTION

High efficiency oscillations in silicon avalanche diodes were first reported in April 1967 by Prager, Chang, and Weisbrod.[1] The new high efficiency mode was shown experimentally to be capable of converting dc to microwave power with efficiency greatly exceeding that predicted for the classical IMPATT mode.[2-4] For example pulsed bias operation with 60 percent efficiency at about 750 MHz was reported.[5] Normal IMPATT operation for this structure would be at about 4 GHz with perhaps 10 percent efficiency.

The first theoretical calculation[6] of the high efficiency mode was obtained by computer simulation of carefully characterized experimental results[7] on germanium structures. Pulsed bias operation, with output power of 7.5 watts at 2.6 GHz with efficiency of 40 percent was reported.[8] The mode of oscillation was named TRAPATT, for TRApped Plasma Avalanche Triggered Transit, which describes the new physical mechanisms discovered by the computer simulations.

Characterization of experimental circuits[9] which support TRAPATT oscillations and additional more detailed simulations[10] of the diode-circuit system further verify the avalanche-triggered-trapped plasma description of the high efficiency mode.

In this paper a simplified model, previously described,[11,12] for the physical processes occurring in TRAPATT operation is employed in order to analyze a wide range of structures and operating conditions. Detailed terminal voltage waveforms are calculated, using appropriate ionization rates, velocities, and other materials parameters, for germanium and silicon structures. The avalanche-zone-transit model, first described in Ref. 11, is presented in detail, and in a form suited for the calculation of the detailed spacial variation of carriers and electric field. Analysis of the diode recovery from the "trapped-plasma" state follows the treatment presented in Ref. 12. Solutions are obtained by applying a terminal current waveform with sharp wavefronts appropriately chosen to represent the effects of the multiresonant circuit to the diode terminals.[9,10] A power generating cycle commences with the application of a large terminal current to a completely swept-out diode structure in which the only carriers available for impact ionization result from thermal generation via defect centers. A rapidly moving avalanche zone results which sweeps through the depletion region from the p-n junction to the heavily doped substrate-base interface. A dense electron-hole plasma is left behind the zone and constitutes a high conduction current essentially zero voltage state which lasts for approximately a half period. Recovery to the essentially zero conduction current-high voltage state is also controlled by terminal current waveform. The avalanche zone transit occurs in a time considerably less than the transit time of a carrier moving at saturated velocity. The sweep-out recovery period cannot be less than the transit time.

The TRAPATT phenomena described above cannot exist as a small signal effect. Instead it results as the natural (and ultimate) large signal limit of the chain of events which occur when a sufficiently large drive is applied to a swept-out avalanche diode. Obviously, a wide range of characteristics result over the range from small signal to large signal,

and between single resonance and multiresonance circuits. In this paper, we calculate only results in the range of the TRAPATT large-signal limit. Furthermore, to facilitate comparisons between germanium and silicon semiconductors, structure designs, bias levels, and operating frequencies, we present detailed results for only a particular terminal current waveform. This waveform, however, would be expected to permit the highest power output at a given frequency, and analysis of the output spectrum agrees with experimental circuit characteristics. This waveform is a perfect square wave of terminal current chosen so that the avalanche zone transient and the subsequent sweep-out of the generated electron-hole plasma occurs precisely over the positive half period. The negative half period is one of high reverse voltage and low saturation current.

The next two sections (II and III) are mathematical and develop the expressions* which are evaluated for a wide range of parameters in Section IV. Section II develops in detail the mathematical characteristics of the avalanche zone transient, which occurs when the step in current is applied to a completely swept-out diode. Section III is a development of the mathematical expressions which describe the recovery period back to the completely swept-out state. Section IV contains: (*i*) A summary of the expressions developed in Sections II and III, required for the complete analysis. (Readers not interested in mathematical detail may omit Sections II and III.) (*ii*) A discussion of the structure design which results as a requirement imposed by the particular current waveform. (*iii*) Results of efficiency, input power density, and diode impedance versus operating frequency for two typical structure designs. (*iv*) For particular optimum structures, results of depletion layer thickness, epitaxial impurity concentration, diode junction area, average voltage, average current, and output power versus operating frequency. Section V presents a discussion of these results, and their comparison with experimental information.

II. SIMPLIFIED MODEL FOR ZONE TRANSIENT

Selected frames of a computer simulation,[13] shown in Figs. 1–3 illustrate the zone transit of TRAPATT operation. Shown are solutions for hole and electron concentrations and electric field profiles at successive instants of time. A zone transit begins, as shown in Fig. 1, when a large current charges a previously swept-out diode structure until impact avalanche generation of carriers begins. For circuit conditions,

* The results of the analysis are identical to those presented in Ref. 12, although the derivation follows from a different point of view.

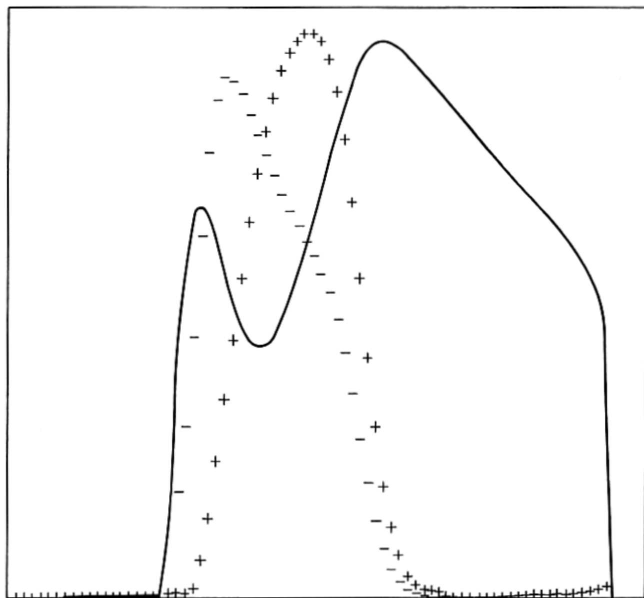

Fig. 1—Start of zone transient. Hole concentration (+), electron concentration (−), electric field (solid) versus distance.

which maintain this large current, the avalanche zone sweeps through the depletion region, as shown in Fig. 2. A dense electron-hole plasma is left, as shown in Fig. 3, after the completion of the zone transit. The computer simulations utilize a model for the semiconductor diode,[5] which is quite general and has been quite successful in simulating large-signal operation of the various modes of power generation in avalanche diodes. Simulated solutions are obtained for the evolution in time of the diode variables (hole and electron concentrations and electric fields) and circuit variables (terminal current and voltage). The main disadvantage of the program is the cost, which generally prohibits a large-scale parameter investigation of the diode-circuit system.

In this section the expressions are derived which form the basis for a large-scale parameter study for the zone transient. The treatment is necessarily simplified, and it is assumed that holes and electrons have identical properties, except for sign, and in particular the ionization rate α and carrier velocity v are identical functions of the electric field $\mathcal{E}$. The one-dimensional continuity, transport, and space-charge equations are simplified to

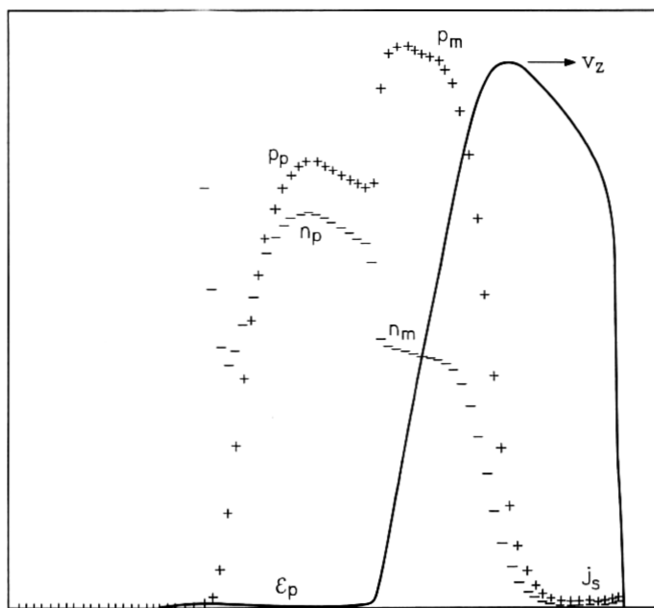

Fig. 2—Zone transient period. Indicated are multiplied carriers p_m and n_m, plasma concentrations p_p and n_p, and plasma field $\mathcal{E}_p$, resulting from initial concentration j_s and zone velocity v_z.

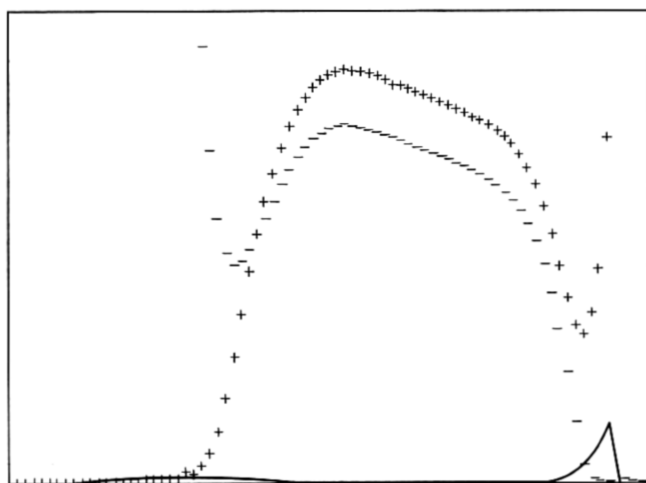

Fig. 3—Termination of zone transient.

$$q \frac{\partial p}{\partial t} = g_T + \alpha(j_p + j_n) - \frac{\partial j_p}{\partial x}, \tag{1}$$

$$q \frac{\partial n}{\partial t} = g_T + \alpha(j_p + j_n) + \frac{\partial j_n}{\partial x}, \tag{2}$$

$$j_p = qvp, \tag{3}$$

$$j_n = qvn, \tag{4}$$

$$\frac{\partial \mathcal{E}}{\partial x} = \frac{q}{\epsilon}(p - n + \text{Dop}), \tag{5}$$

in which diffusion transport has been neglected, g_T represents thermal generation via defects where significant, and Dop is the net ionized impurity concentration.

A reduction in the number of required equations can be obtained by differentiating the space-charge equation and substituting from the expression which results when the two continuity equations are added:

$$\epsilon \frac{\partial}{\partial x}\left(v \frac{\partial \mathcal{E}}{\partial x}\right) = q \frac{\partial}{\partial x}\left(\frac{j_p - j_n}{q} + v \cdot \text{Dop}\right), \tag{6}$$

$$\frac{\partial}{\partial t}\left(\frac{j_p + j_n}{v}\right) = 2g_T + 2\alpha(j_p + j_n) - \frac{\partial}{\partial x}(j_p - j_n) \tag{7}$$

or

$$\epsilon \frac{\partial}{\partial x}\left(v \frac{\partial \mathcal{E}}{\partial x}\right) = q \frac{\partial}{\partial x}(v \cdot \text{Dop}) + 2g_T + 2\alpha j_c - \frac{\partial}{\partial t}\left(\frac{j_c}{v}\right) \tag{8}$$

where j_c is the conduction current ($j_c = j_p + j_n$) and

$$j_c = J_T - \epsilon \frac{\partial \mathcal{E}}{\partial t}, \tag{9}$$

where J_T is terminal current density.

A single equation in $\mathcal{E}$ results by substituting equation (9) into (8), but is of no particular advantage. The solution for $\mathcal{E}$ and j_c is instead obtained from the following two equations, where doping gradients have been neglected:

$$\frac{\partial j_c}{\partial t} = 2v(g_T + \alpha j_c) + \frac{j_c v'}{\epsilon v}(J_T - j_c) - \epsilon v^2 \frac{\partial^2 \mathcal{E}}{\partial x^2} + vv' \frac{\partial \mathcal{E}}{\partial x}\left(q\,\text{Dop} - \epsilon \frac{\partial \mathcal{E}}{\partial x}\right), \tag{10}$$

$$\epsilon \frac{\partial \mathcal{E}}{\partial t} = J_T - j_c\,. \tag{11}$$

Equation (10) is obtained from equation (8) by expressing $\partial v/\partial x$ in terms of an incremental mobility $v' = dv/d\mathcal{E}$, that is, $\partial v/\partial x = v' (\partial \mathcal{E}/\partial x)$, and $(\partial v/\partial t) = v'(\partial \mathcal{E}/\partial t)$.

2.1 *Coordinate Transformation*

The zone transient period of a TRAPATT oscillation is distinctively characterized by the rapid movement of an avalanche zone from the p-n junction to the base-substrate interface,[11,12] in which computer simulations[6,10,13] indicate that all quantities at a time $t_0 + \Delta t$ have profiles related to those existing at time t_0, by the relationship

$$\mathcal{E}(x, t_0 + \Delta t) = \mathcal{E}(x - v_z \Delta t, t_0),$$

where the electric field is used for illustration. Incorporation of this "experimentally" observed phenomena into the mathematical model results in the elimination of all partial derivatives with respect to time, and replacing them with an ordinary special derivative. That is by making a change of variable $z = x - v_z \cdot \Delta t$,

$$\frac{\partial}{\partial t} \rightarrow -v_z \frac{d}{dz} \tag{12}$$

where v_z is the velocity of the zone and is assumed constant. Incorporation of transformation (12) into equations (10) and (11) yields

$$\frac{v_z}{v_s} \frac{dj_c}{dz} = \epsilon v_s \frac{d^2 \mathcal{E}}{dz^2} - 2v_s(g_T + \alpha j_c) \tag{13}$$

and

$$-\epsilon v_z \frac{d\mathcal{E}}{dz} = J_T - j_c, \tag{14}$$

for the case where the velocity is saturated at value v_s. The velocity of the zone is readily obtained[11,12] from equation (14), when evaluated in the region in front of the avalanche, where $j_c \ll J_T$ and $d\mathcal{E}/dz = -(q/\epsilon)N_A$: $v_z = J_T/qN_A$. If thermal generation is neglected, once the avalanche zone is formed, equations (13) and (14) can be separated and integrated to yield the detailed structure of the avalanche zone for any $\alpha(\mathcal{E})$ function, and most interestingly predicts the magnitude of multiplication of conduction current through the zone—independent of the exact form of the $\alpha(\mathcal{E})$ function: Substitution into equation (13) of the derivative of equation (14) with respect to z yields

$$2\alpha j_c = \left(\frac{v_s}{v_z} - \frac{v_z}{v_s}\right) \frac{dj_c}{dz}. \tag{15}$$

Further substitution of dz from equation (14) yields

$$2\alpha j_c = \left(\frac{v_s}{v_z} - \frac{v_z}{v_s}\right)\frac{dj_c}{d\mathcal{E}}\left(\frac{j_c - J_T}{\epsilon v_z}\right),$$

which can be rearranged as

$$2\epsilon v_z \alpha(\mathcal{E})\, d\mathcal{E} = \left(\frac{v_s}{v_z} - \frac{v_z}{v_s}\right)\left(\frac{j_c - J_T}{j_c}\right) dj_c\,. \tag{16}$$

With the condition that the conduction current in front of the zone has constant value j_s (as a result of thermal generation during the previous clear-out sequence), the relationship between value of electric field in the zone and conduction current is given by

$$\epsilon \int_0^{\mathcal{E}(j_c)} \alpha(\mathcal{E})\, d\mathcal{E} = \left(\frac{v_z}{v_s} - \frac{v_s}{v_z}\right)\left[J_T \ln\left(\frac{j_c}{j_s}\right) - j_c + j_s\right] \Big/ (2v_z)\cdot \tag{17}$$

From equation (15) we see that v_z must be greater than v_s in order to multiply up conduction current from the value j_s . The total current multiplication j_{cm} across the entire zone is obtained by evaluating the upper limit of the left side of equation (17) also at zero field, in which case the left side equals zero and j_{cm} is given by

$$j_{cm} = j_s e^{(j_{cm} - j_s / J_T)}, \tag{18}$$

which shows that the effect of an increase in j_s , is a decrease in j_{cm} .[11]

2.2 *Individual Hole and Electron Concentrations*

The individual hole and electron concentrations can be obtained from the value of j_c . The expressions are derived for two regions. One is anywhere within the zone where $v = v_s$, and the other is to the left of the zone where v may be less than v_s .

For $v = v_s$:

$$j_c = qv_s(p + n),$$

which can be solved simultaneously with

$$\frac{q}{\epsilon}(p - n - N_A) = \frac{j_c - J_T}{\epsilon v_z},$$

obtained by equating equations (5) and (14), as

$$p = \frac{j_c}{2q}\left(\frac{1}{v_s} + \frac{1}{v_z}\right); \tag{19}$$

$$n = \frac{j_c}{2q}\left(\frac{1}{v_s} - \frac{1}{v_z}\right). \tag{20}$$

Therefore if the detailed variation of j_c is determined, for a particular $\alpha(\mathcal{E})$ function, from equation (17), equations (19) and (20) yield the detailed profiles of carriers through the zone. In particular the values of holes and electrons, see Fig. 2, when $j_c = j_{cm}$ are simply

$$p_m = \frac{j_{cm}}{2q}\left(\frac{1}{v_s} + \frac{1}{v_z}\right), \tag{21}$$

$$n_m = \frac{j_{cm}}{2q}\left(\frac{1}{v_s} - \frac{1}{v_z}\right). \tag{22}$$

2.3 *For* $v \leqq v_s$:

In this region impact ionization can be neglected and we return to the individual hole and electron continuity equations (1) and (2) written as

$$-v_z \frac{dp}{dz} = -\frac{d}{dz}(pv), \tag{23}$$

$$-v_z \frac{dn}{dz} = \frac{d}{dz}(nv), \tag{24}$$

where v is the carrier drift velocity. Inspection of the above equations reveals that any solution must satisfy the following constraints:

$$c_p = p(v_z - v), \tag{25}$$

$$c_n = n(v_z + v), \tag{26}$$

where c_p and c_n are constants. The validity of equations (25) and (26) can be checked by differentiation.

The value of c_p and c_n can be obtained by substitution of p_m and n_m from equations (21) and (22), and reveals that $c_p = c_n = c$:

$$c = \frac{j_{cm}}{2q}\left(\frac{v_z}{v_s} - \frac{v_s}{v_z}\right). \tag{27}$$

The values of p and n for any $v \leqq v_s$ are given by

$$p = \frac{j_{cm}}{2q}\left(\frac{v_z}{v_s} - \frac{v_s}{v_z}\right) \Big/ (v_z - v(\mathcal{E})), \tag{28}$$

$$n = \frac{j_{cm}}{2q}\left(\frac{v_z}{v_s} - \frac{v_s}{v_z}\right) \Big/ (v_z + v(\mathcal{E})). \tag{29}$$

2.4 *Trapped Plasma Solution*

The profiles of holes, electrons and field in the transition region over which the carriers change from values p_m and n_m to their values in the trapped plasma, p_p and n_p, can be obtained from the simultaneous solution of equations (28) and (29) and equation (14) for any arbitrary $v(\mathcal{E})$ relation. However the solution in the trapped plasma is independent of the exact form of $v(\mathcal{E})$, and the plasma concentration of holes and electrons is even independent of the value of low field mobility.

In the trapped plasma the values of holes, electrons, and field (p_p, n_p, and $\mathcal{E}_p$) are related by

$$p_p - n_p = N_A , \tag{30}$$

$$J_T = qv_p(p_p + n_p), \tag{31}$$

$$v_p = \mu \mathcal{E}_p . \tag{32}$$

The solution for v_p is obtained from equations (28), (29) and (30):

$$v_p = \frac{j_{cm}}{2qN_a}\left(\frac{v_z}{v_s} - \frac{v_s}{v_z}\right)\left\{\left[1 + \left[\frac{2qN_a v_z}{j_{cm}\left(\frac{v_z}{v_s} - \frac{v_s}{v_z}\right)}\right]^2\right]^{\frac{1}{2}} - 1\right\}. \tag{33}$$

Once v_p is found, the values of p_p and n_p are given by

$$p_p = \frac{N_A}{2}\left(\frac{v_z}{v_p} + 1\right), \tag{34}$$

$$n_p = \frac{N_A}{2}\left(\frac{v_z}{v_p} - 1\right). \tag{35}$$

2.5 *Discussion of Zone Transient*

A simplified model for the zone transient which results from the transformation, equation (12), has been presented. In the numerical analysis the calculation begins at the point where the electric field is a maximum and $j_c = J_T$. Solutions are then obtained by the simultaneous solution of equations (16) and (14) for j_c and $\mathcal{E}$ as functions of position to the left and to the right of this point. The hole and electron profiles are then obtained from equations (19) and (20). The value of plasma velocity v_p is obtained from a solution of equation (33), and the plasma density from equations (34) and (35).

It is of great significance to note that the solution in the trapped plasma is independent of the exact form of the $\alpha(\mathcal{E})$ and $v(\mathcal{E})$ relations and is determined uniquely by the value of j_s, N_A, and J_T.

A simplification for the trapped plasma solution results for the condi-

tion $v_p \ll v_z$. Equations (33), (34) and (35):

$$\frac{v_p}{v_z} = \frac{J_T}{j_{cm}\left(\frac{v_z}{v_s} - \frac{v_s}{v_z}\right)}, \quad (36)$$

$$p_p = \frac{N_A}{2}\left(\frac{j_{cm}}{J_T}\left(\frac{v_z}{v_s} - \frac{v_s}{v_z}\right) + 1\right), \quad (37)$$

$$n_p = \frac{N_A}{2}\left(\frac{j_{cm}}{J_T}\left(\frac{v_z}{v_s} - \frac{v_s}{v_z}\right) - 1\right). \quad (38)$$

In the next section we present an analysis of the recovery period of the diode from the trapped plasma state to the state in which the diode is completely free (except for thermal generation) of mobile carriers.

III. RECOVERY TRANSIENT

In this section the transient solution is calculated for a plasma filled n^+pp^+ diode after the application of constant reverse bias current J_R , which is a good approximation to the recovery portion of a TRAPATT oscillation. The analysis also applies to the devices treated by Benda and Spenke for the reverse recovery in power rectifiers,[14] and by Moll and Hamilton for step recovery diodes.[15] However, the recovery from the large density plasma to a swept out state of large voltage, which occurs in TRAPATT operation, differs substantially from the earlier treatment[14,15] which applies to low density plasmas and slow removal rates.

It is found that the removal rate of the electron-hole plasma and build-up of the electric field profile is quite accurately described by a simple model[12] which includes the effects of displacement current and carrier drift at constant mobility and saturated velocity. For a given p-region width the total recovery time can be as small as the transit time of the slower carrier if the plasma density is less than a critical value and the reverse current equals a critical value. For current greater than a critical value avalanche occurs before complete carrier removal. The first part of this section pertains to a more general system in which holes and electrons are not required to have equal characteristics; while the second part is for the special case of equal properties and couples the zone transient analysis with the recovery analysis.

3.1 *Part 1*

Figures 4a and 4b are frames from a computer simulation run to test the analysis to follow and will serve for notation.

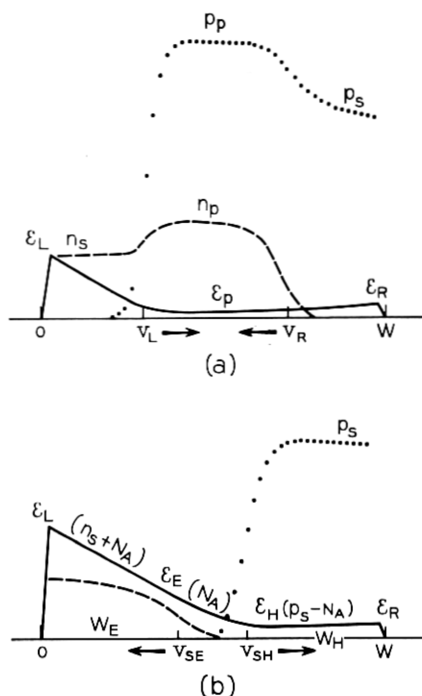

Fig. 4—Recovery transient. Hole concentration, electron concentration, and electric field versus distance. (a) Plasma velocity period and (b) saturated velocity period.

At $t = 0$ the diode has a uniform plasma p_p and n_p and the center region is characterized by:

$$p_p = N_A + n_p ,$$

$$J_R = q\mathcal{E}_p(\mu_p p_p + \mu_n n_p),$$

where $\mathcal{E}_p$ is the field in the plasma μ_p and μ_n the hole and electron mobilities, and J_R the reverse or recovery current.

The solution for carrier density p_s , n_s and velocities v_L and v_R^* is obtained by an integration of the continuity equations over the transition region from the plasma to the regions where the field has built up to that required for saturated velocity:

$$q \frac{\partial}{\partial t} \int p \, dx = -\int dj_p$$

* v_L and v_R are the hole and electron velocities, respectively, in the plasma.

and

$$q \frac{\partial}{\partial t} \int n \, dx = \int dj_n$$

or

$$(p_p - p_s)v_R = v_{SH}p_s - \mu_p p_p \mathcal{E}_p ,$$
$$(n_p - n_s)v_L = v_{SE}n_s - \mu_n p_p \mathcal{E}_p ,$$
$$n_p v_R = \mu_n \mathcal{E}_p n_p ,$$
$$p_p v_L = \mu_p \mathcal{E}_p p_p .$$

From the relations above:

$$v_R = \mu_n \mathcal{E}_p , \tag{39}$$

$$v_L = \mu_p \mathcal{E}_p , \tag{40}$$

$$p_s = p_p \frac{(v_R + v_L)}{(v_R + v_{SH})} , \tag{41}$$

$$n_s = n_p \frac{(v_L + v_R)}{(v_L + v_{SE})} , \tag{42}$$

where v_{SH} and v_{SE} are the saturated hole and electron velocities. The solution as shown in Fig. 4a, with values for v_L , v_R , p_s , n_s as given above (and verified by computer simulations), is valid until a time t_0 , when the plane moving at velocity v_L reaches the plane moving at velocity v_R :

$$t_0 = W/(v_R + v_L). \tag{43}$$

For $t \leqq t_0$ the terminal voltage is given by

$$V = \frac{q}{\epsilon} \frac{t^2}{2} [v_R^2 p_S + v_L^2 n_S + N_A(v_L^2 - v_R^2)]. \tag{44}$$

For the remainder of the clear-out cycle refer to Fig. 4b. For times greater than t_0 three regions exist:

Region 1 extends from $x = 0$ to the plane moving at velocity v_{SE} . The field here has slope given by

$$\frac{\partial \mathcal{E}}{\partial x} = -\frac{q}{\epsilon} (N_A + n_s), \tag{45}$$

and the field $\mathcal{E}_L$ has a magnitude given by

$$\epsilon \mathcal{E}_L / t = J_R - q v_{SE} n_s = q v_L (n_s + N_A) \tag{46}$$

Region 3 extending from the plane moving at velocity v_{SH} to $x = W$. The field here has slope given by

$$\frac{\partial \mathcal{E}}{\partial x} = \frac{q}{\epsilon}(p_s - N_A), \tag{47}$$

and the field $\mathcal{E}_R$ has a magnitude given by

$$\epsilon \mathcal{E}_R/t = J_R - qv_{SH}p_s = qv_R(p_s - N_A). \tag{48}$$

Region 2, the remainder, has electric field with slope

$$\frac{\partial \mathcal{E}}{\partial x} = -\frac{q}{\epsilon} N_A . \tag{49}$$

The terminal voltage V for $t \geqq t_0$ is obtained, with reference to Fig. 4b as follows.

$$\begin{aligned} V &= (\mathcal{E}_L + \mathcal{E}_E)/2 \cdot W_E , \\ &+ (\mathcal{E}_R + \mathcal{E}_H)/2 \cdot W_H , \\ &+ (\mathcal{E}_E + \mathcal{E}_H)/2 \cdot (W - W_E - W_H), \end{aligned}$$

or rearranged as

$$V = \tfrac{1}{2}[\mathcal{E}_L W_E + \mathcal{E}_R W_H + \mathcal{E}_E(W - W_H) + \mathcal{E}_H(W - W_E)], \tag{50}$$

where

$$\begin{aligned} W_E &= v_L t_0 - v_{SE}(t - t_0), \\ W_H &= v_R t_0 - v_{SH}(t - t_0) \end{aligned}$$

$\mathcal{E}_E$ and $\mathcal{E}_H$ are given by equations (46) and (48) and

$$\mathcal{E}_E = \mathcal{E}_L - \frac{q}{\epsilon}(N_A + n_s)W_E ,$$

$$\mathcal{E}_H = \mathcal{E}_R - \frac{q}{\epsilon}(p_s - N_A)W_H .$$

Equation (50) is valid until W_E or W_H equals zero, the time required to completely remove electrons or holes. The times required to completely clear-out electrons and holes are

$$\Delta t_E = \frac{W}{v_{SE}} \frac{n_p}{n_s} , \tag{51}$$

$$\Delta t_H = \frac{W}{v_{SH}} \frac{p_p}{p_s} , \tag{52}$$

where p_s and n_s are given by equations (41) and (42).

3.2 *Minimum Recovery Time*

If the recovery current J_R is chosen so that $v_R = v_{SE}$ and $v_L = v_{SH}$, that is,

$$J_R = q(v_{SH}p_p + v_{SE}n_p) \equiv J_c , \tag{53}$$

the clear-out will proceed at its most rapid rate. Any further increase in J_R will not speed up the recovery but will result in a $\partial\mathcal{E}/\partial t$ in the plasma which will result in an unnecessarily large value of $\mathcal{E}_L$ or $\mathcal{E}_R$ near the end of the recovery period and premature avalanche before clear-out. For $J_R = J_c$:

$$p_s = p_p ,$$

$$n_s = n_p .$$

A constraint on p_p is obtained by requiring the field $\mathcal{E}_L$ (obtained from equation (46) with $J_R = J_c$) to be less than the value obtained there in steady-state breakdown $\mathcal{E}_0$, that is,

$$p_p < \epsilon\mathcal{E}_0/qW, \tag{54}$$

for $t = \Delta t_H$. Since $p_p > N_A$, equation (54) indicates that the diode must have a punch-through voltage less than the breakdown voltage. The computer simulation shown in Fig. 4 is for silicon with equal properties assumed for holes and electrons at 300°K, $W = 10$ microns, $p_p = 1.52 \times 10^{15}$, $n_p = 0.514 \times 10^{15}$, $N_A = 1.0 \times 10^{15}$, and $J_R = 1.5 \times 10^3\ A/\text{cm}^2$.

3.3 *Part II*

For the remainder of this section it is assumed that holes and electrons have equal properties and therefore only one plasma velocity v_p replaces v_R and v_L , and one saturated velocity v_S replaces v_{SE} and v_{SH} in the previous equations. Furthermore, the plasma velocity obtained during the zone-transit period while current J_T flows is not the same as the plasma velocity characteristic of the recovery period while current J_R flows; unless $J_T = J_R$. Therefore the following notation is used:

v_{PT} = velocity of plasma while current J_T flows,

v_{PR} = velocity of plasma while current J_R flows.

A factor F is defined by reference to Fig. 5. The breakdown voltage of the diode is V_0 , the field at the n^+p junction at breakdown is $\mathcal{E}_0$, and

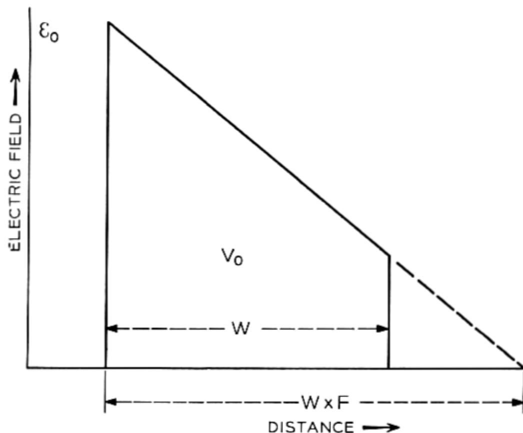

Fig. 5—Definition of punch-through factor F. Electric field versus distance at breakdown.

the width of the depletion region is smaller than the value $\epsilon\mathcal{E}_0/qN_A$ by a factor $F > 1$. That is F is a measure of the degree of punch-through. (In the numerical calculation $\mathcal{E}_0$ and W are obtained by an iterative process for any given value of N_A and F.)

It is the purpose of this section to derive design requirements for TRAPATT operation by coupling the zone-transit analysis and the recovery analysis. It will be shown that the value of recovery current J_R which will result in complete removal of the plasma just as the diode voltage (and field profile) are the breakdown values V_0 and $\mathcal{E}_0$ is,

$$J_R = qN_A v_S(2F - 1);$$

and for the condition that the plasma be extracted in one transit time the following constraint must be imposed on the zone transit:

$$v_z/v_{PT} = 2F - 1.$$

The above constraint yields a unique value for J_T, for any given structure. This value is uniquely determined by material (Ge or Si), N_A, F, and J_S. For an additional constraint, for example that we minimize the sum of zone-transit time and recovery time or that this time period have a fixed relationship to the IMPATT transit time, a unique value of F can be determined. By such constraints then a unique (except for weak dependence on J_S) power-versus-frequency curve can be obtained for a given material. The derivation of the expressions required follows.

At the end of the zone transit the diode has plasma density given by equations (34) and (35). The clear-out densities p_s and n_s are

$$p_s = N_A\left(\frac{v_z}{v_{PT}} + 1\right)\frac{v_{PR}}{v_{PR} + v_s}, \tag{55}$$

$$n_s = N_A\left(\frac{v_z}{v_{PT}} - 1\right)\frac{v_{PR}}{v_{PR} + v_s}. \tag{56}$$

Utilizing equations (55) and (52) the electric field $\mathcal{E}_L$, obtained from equation (46), just as the carriers are cleared out has value

$$\mathcal{E}_L(\Delta t) = qv_{PR}(n_s + N_A)\left(\frac{Wp_p}{\epsilon v_s p_s}\right),$$

and when set equal to $\mathcal{E}_0$ (from Fig. 5 $\mathcal{E}_0 = (q/\epsilon)N_AFW$) yields

$$(n_s + N_A)\frac{v_{PR}P_p}{v_sP_s} = N_AF.$$

Further substitution from equations (41) and (56) yields

$$2F = 1 + \frac{v_z}{v_s}\left(\frac{v_{PR}}{v_{PT}}\right)$$

or utilizing equations (41) and (42)

$$J_R = qN_Av_s(2F - 1). \tag{57}$$

The equation above results solely from the requirement that right when the last remnants of the plasma are leaving the depletion region, the diode is at breakdown voltage V_0. We have the interesting result that the degree of punch-through (F) *uniquely* determines—an upper limit on the reverse recovery current, independent of the zone transit current J_T, ionization rate, mobility or saturation current.

The critical current for removal of the plasma in one transit time is

$$J_c = qv_s(p_p + n_p).$$

For p_p and n_p given by equations (34) and (35),

$$J_c = qv_sN_Av_z/v_{PT},$$

and for the condition $J_R = J_c$,

$$\frac{v_z}{v_{PT}} = 2F - 1. \tag{58}$$

Equation (58) imposes a constraint on the zone transit process so that

the resulting plasma can be removed in one transit time. From the zone-transit analysis, in particular equation (33), a relationship was derived relating v_z, v_s, j_{cm}, N_A and v_{PT}. Therefore, combining equations (33) and (58) yields a relationship between F, N_A, v_s, J_T and j_s, which must be satisfied if the plasma is to be extracted in one transit time. However, the condition for maximum frequency is one which minimizes the sum of three characteristic times: the charging time t_1, the zone transit time t_2 and the recovery time (compare Fig. 6).

The power output of an avalanche diode is limited by realizable circuit impedance or thermal limitations. Both have the effect of limiting the area of the diode. For a given upper limit on circuit impedance the best design is one which maximizes the product of power output times frequency squared. This figure of merit (F.M.) will have a maximum value determined by a judicious choice for J_T, J_R, the duration of time they are applied, and the duration of time the breakdown voltage-saturation current state persists. Such optimum conditions are not sought in the present analysis, inasmuch as after they were found it would probably be quite difficult to design a realistic circuit which could provide such a waveform. Instead, optimum values of F and current amplitude are found such that the F.M. is a maximum for perfect square wave current drive. (This is experimentally observed[10] where the square wave is made up of a limited number of odd harmonics; the circuit is an open circuit at all even harmonics,

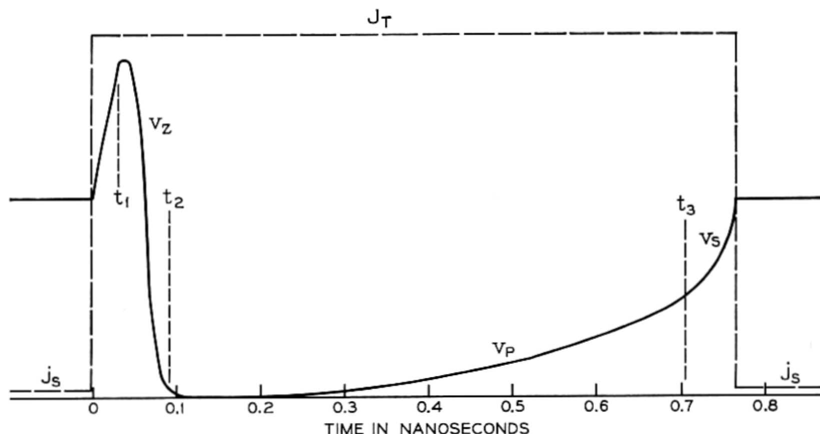

Fig. 6—Example of calculated voltage (solid) and assumed diode current (dashed) versus time. Zone transit (v_z), plasma velocity recovery (v_p), and saturated velocity (v_s), periods indicated.

the fundamental has impedance as calculated herein, and the third harmonic corresponds to the IMPATT frequency.) The next section reports results of a calculation for such a power-frequency characteristic.

IV. POWER OUTPUT AND STRUCTURE DESIGN

The application of terminal current J_T to a swept-out diode results in the zone transients shown in Figs. 1–3. In Section II we presented a considerably simplified analysis for the zone transient, as shown for example in Fig. 2. In Section III we analyzed the recovery transient, as shown in Figs. 4. A recovery current $J_R = qN_A v_s (2F - 1)$, equation (57), is required to completely remove the plasma in as short a time as possible, such that the diode voltage and field profile have just attained the breakdown values. The structure factor F and breakdown values are defined by Fig. 5. In the first part of this section results are presented on a per unit area basis. The voltage waveform, as shown for example in Fig. 6, is calculated for various values of N_A, ranging from 10^{15} cm^{-3} to 10^{17} cm^{-3}, and values of F equal to 1.5 and 2.0. The current density J_T is determined by equation (57). The resulting waveform is Fourier analyzed, the frequency determined, and results presented in Figs. 7–9. In the second part, results are presented for an optimally chosen structure: (*i*) The value of F is found for each value of N_A such that the ratio of IMPATT frequency (π transit angle) to TRAPATT frequency is 3 : 1. (*ii*) The diode area is chosen to provide 10 ohms negative resistance, a reasonable value for microwave circuits. These results are presented in Figs. 10–15.

4.1 *Part I*

As shown in Section II the zone transient solution is logarithmically related to the thermally generated current j_s. In the calculations the current j_s is given by

$$j_s = qn_i W/\tau. \tag{59}$$

The intrinsic carrier concentration is evaluated at 300°C. for silicon and 100°C. for germanium, and the lifetime τ is 100 nsec. Effects of variations of j_s on device design are considered elsewhere.[12] The saturated velocity v_s is 8.9×10^6 cm/sec for silicon and 6.5×10^6 cm/sec for germanium. The ionization rate $\alpha = ae^{-b/E}$ has a and b 1.6×10^6 cm^{-1}, 1.9×10^6 V/cm for silicon and 3.5×10^5 cm^{-1}, 7.5×10^5 V/cm for germanium.[16]

The waveform of diode voltage for a particular structure is shown

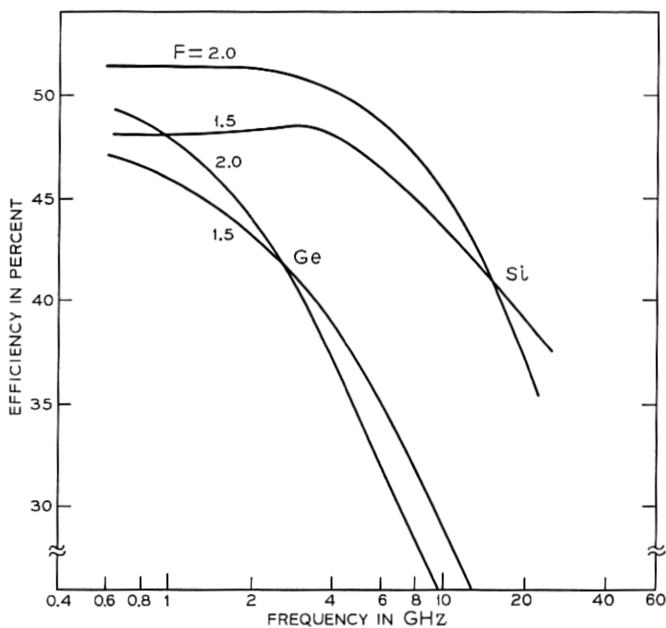

Fig. 7—Efficiency versus frequency, $F = 1.5$ and 2.0.

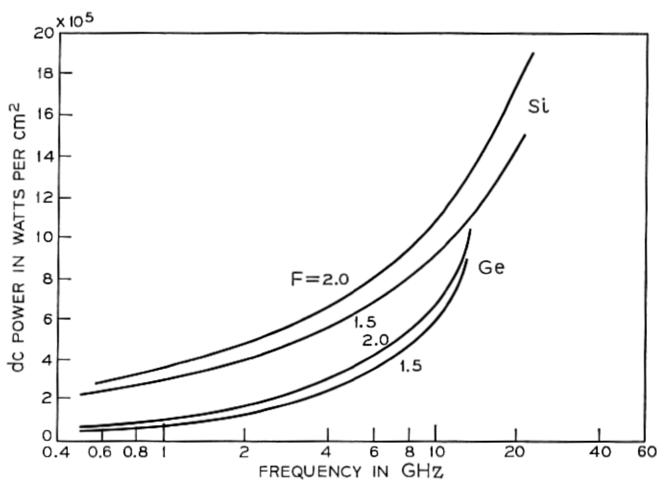

Fig. 8—Input (average) power density versus frequency, $F = 1.5$ and 2.0.

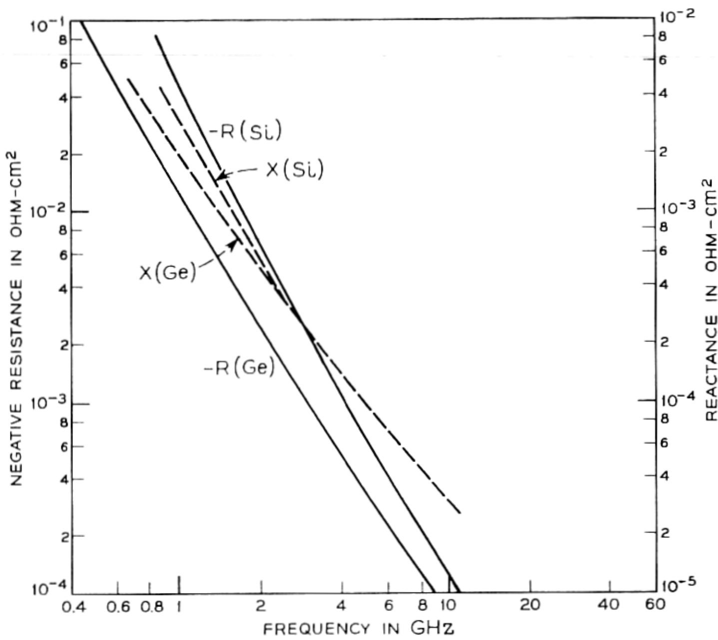

Fig. 9—Diode impedance versus frequency, $F = 1.5$.

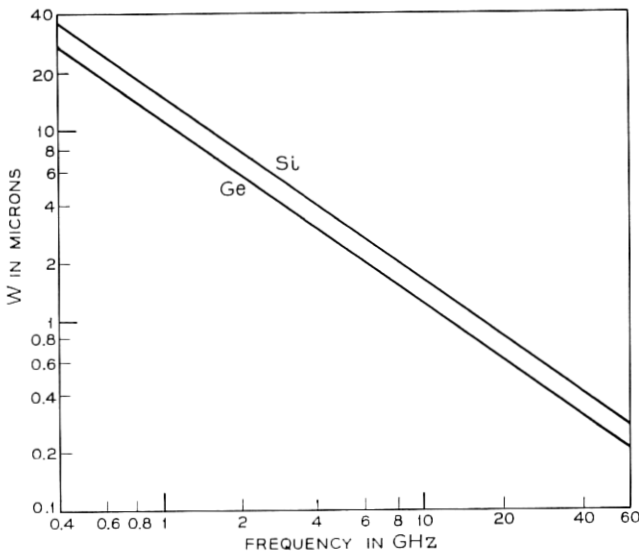

Fig. 10—Depletion layer thickness W versus frequency.

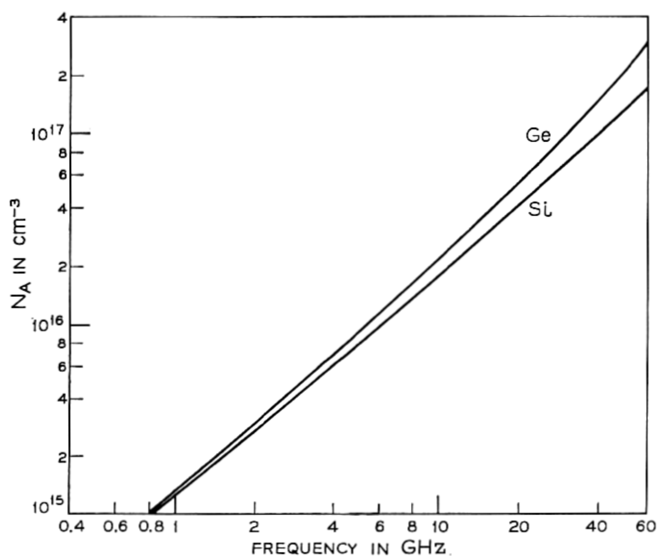

Fig. 11—Impurity concentration N_A versus frequency.

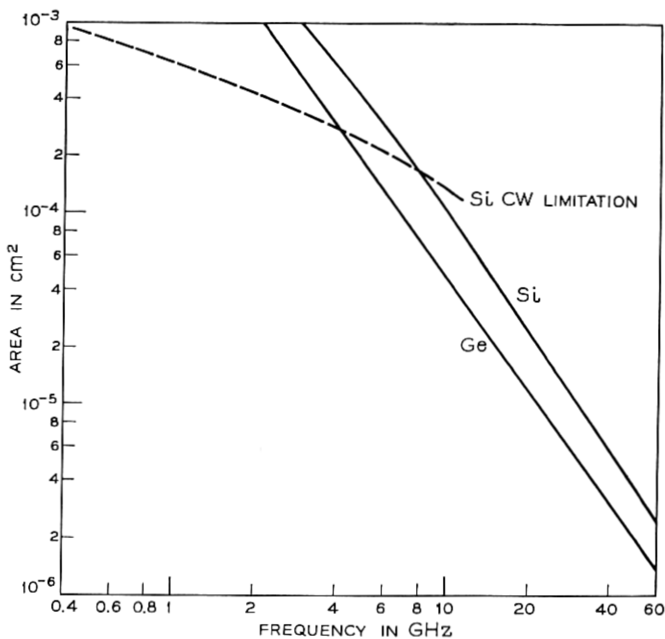

Fig. 12—Diode area versus frequency.

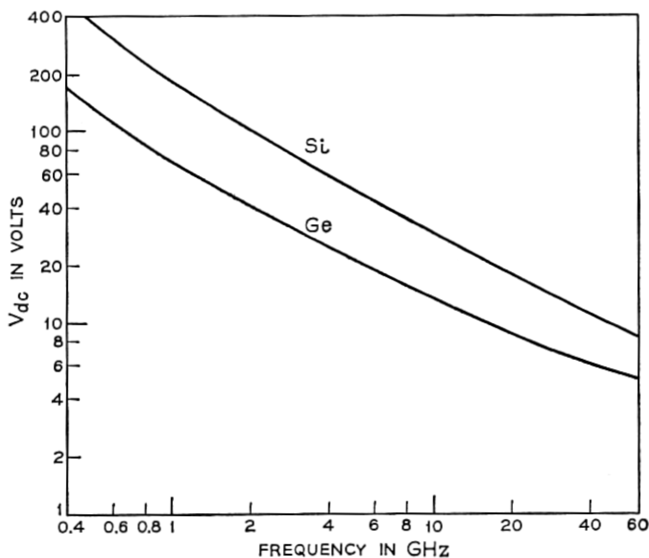

Fig. 13—Average voltage versus frequency.

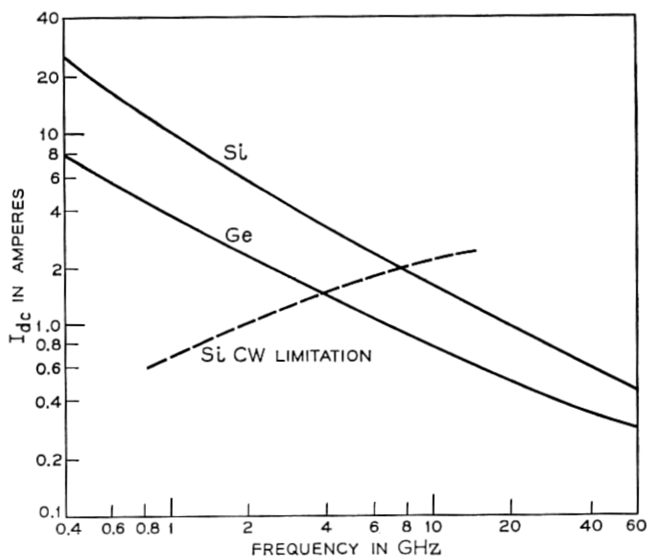

Fig. 14—Average current versus frequency.

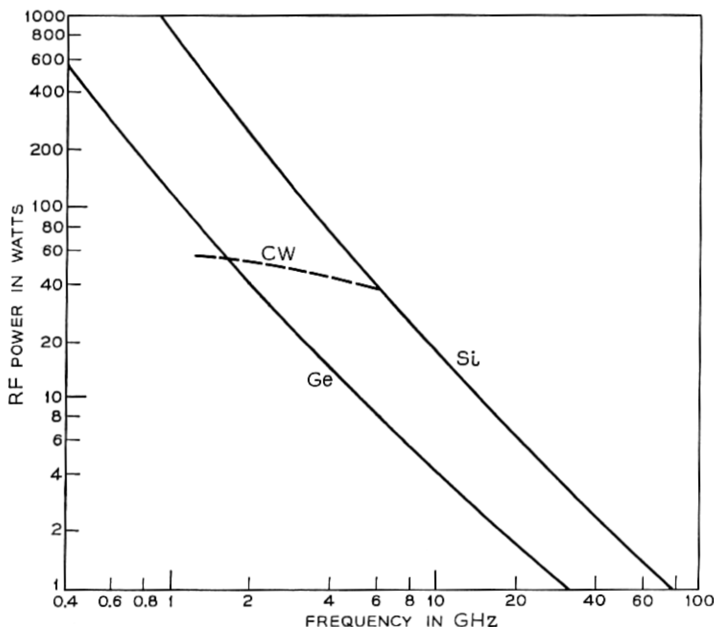

Fig. 15—Output power versus frequency.

in Fig. 6. The time t_1 is a depletion layer capacitance charging time, required to overdrive the diode to the point at which the avalanche zone transient begins. The zone transient lasts until time t_2 . The recovery transient characterized by the plasma velocity v_p lasts until time t_3 . The remainder of the recovery time, to t_4 , is characterized by carriers moving at saturated velocity. After complete sweep-out of carriers, the diode voltage equals the breakdown value and the diode current equals the saturation value j_s , for a half period of duration t_4 .

The voltage waveforms are calculated according to the simplified models presented in Sections II and III. The voltage for times between t_1 and t_2 , the zone transient, are calculated by "sliding" the field profile, shown for example in Fig. 2, from the point where the maximum field occurs at the N^+P junction, corresponding to time t_1 , to the right at velocity v_z . The time t_2 corresponds to the time when the location of the right-most point of the plasma region would enter the substrate. The voltage is the area under the field curve, within the confines of the depletion region. The voltage thus calculated is only an approximation at the beginning of this transient. However, the value of trapped

plasma left in the depletion region at time t_2 is independent of the actual avalanching conditions, and this plasma constitutes the initial conditions for the recovery voltage waveforms from time t_2 until t_4. The voltage waveform in the neighborhood of time t_1 is determined by complicated space charge effects shown in Fig. 1. It is felt that detail occurring over such a short period of time would not significantly affect the overall power output and efficiency calculation, but this is one of the major limitations of this simplified analysis.

Results for two values of punch-through factor F are shown in Figs. 7 and 8. The frequency is calculated (for particular values of N_A) and results shown versus frequency. Figure 7 is a plot of calculated power conversion efficiency versus frequency; Fig. 8, dc power density versus output frequency. The diode impedance, as calculated by Fourier analysis of the waveforms, is shown in Fig. 9 for $F = 1.5$.

4.2 *Part II*

Results shown in Figs. 7–9 are on a per unit area basis, and no optimization for the F factor has been attempted. The area of an avalanche oscillator is determined by circuit impedance limitations and thermal dissipation limitations for CW operation. Results of the calculation are presented in Figs. 10–15 for an area chosen such that 10 ohms negative resistance at the TRAPATT frequency is obtained. In addition, the F factor was chosen by an iterative process for optimization of the diode structure. Initially optimization was sought for the criterion of maximization of the products of output power times operating frequency squared. Results clearly indicated that the maximum was for values of F only slightly larger than 1.0. For such cases the recovery time is very nearly one transit time, the minimum value. The total half period of the oscillation would be only slightly larger than two transit times, and therefore a ratio of IMPATT-to-TRAPATT frequency of 2 : 1 could be obtained. Instead results for a frequency ratio of 3 : 1 are presented. This will be somewhat less than the optimum, but more realistic, as this mode of operation is more easily obtained experimentally.[9,10]

Device depletion layer thickness W, epitaxial impurity concentration N_A, and device area A, calculated for the 3 : 1 mode, are shown in Figs. 10–12, versus output frequency. Operating characteristics are presented in Figs. 13–15. Plotted versus frequency are average voltage, average current, and output power. As discussed previously, device area was chosen to provide 10 ohms negative resistance at the operating (TRAPATT) frequency. No other circuit limitations on area are in-

cluded, such as might be imposed by IMPATT considerations. Such considerations will be discussed later. The output power calculated for a silicon device, if the area is chosen for CW operation, is shown as a dashed line in Fig. 15. The choice of maximum device area permitting CW operation was obtained from silicon IMPATT diode thermal resistance and burnout analysis collected over the past several years at this laboratory.[17] Based on this analysis, circuit impedance limitations determine device area for operating frequencies above about 10 GHz. In addition, device area may have to be reduced to provide sufficient negative resistance to overcome losses at the IMPATT frequency. This effect has not been considered in the present analysis.

V. DISCUSSION

We have presented calculated operating characteristics of the TRAPATT mode of high efficiency power generation in germanium and silicon avalanche diodes. The calculated results were obtained by analysis of solutions of a simplified model for the avalanche zone transit and reverse recovery periods which characterize the TRAPATT mode. The calculated solutions agree well with solutions obtained by detailed computer simulation studies, except for detail missing at the beginning of the zone transit, as the avalanche zone is forming.

Characteristics were presented, on a per unit area basis, for diodes with two degrees of punch-through, of the electric field at breakdown, into the terminating substrate. The silicon structures are more efficient than the germanium but require considerably more input power. For both materials input power requirements increase with F, the degree of punch-through, at a particular frequency.

A particular design was obtained by choosing F such that the TRAPATT frequency would be one-third the IMPATT (π transit angle) frequency of the structure. The calculated epitaxial impurity concentration and depletion layer width were presented. The calculated results are in excellent agreement with our experimental Ge structure ($f = 2.4$ GHz, $W = 4.5\ \mu$m, $N_a = 4.2 \times 10^{15}$ cm^{-3}).[8,10] Calculated results of power output versus frequency were presented for diode areas chosen to yield 10 ohms negative resistance at the TRAPATT frequency, and for silicon diodes with areas determined by thermal limitations. Power output in excess of 1 watt CW, with efficiency of 40 percent is predicted at a frequency of 50 GHz.

VI. ACKNOWLEDGMENTS

The work presented here evolved from computer simulations utilizing a detailed semiconductor program developed by the author and H. K. Gummel, and from the careful experimental characterization of TRAPATT waveforms by R. L. Johnston and precise circuit characterization by W. J. Evans. The author gratefully acknowledges many discussions with those named above and D. J. Bartelink, B. C. DeLoach, Jr., and R. M. Ryder, in which the understanding of the TRAPATT modes developed. The analytical treatments of the avalanche zone and reverse recovery transients, in part or in total, has been carefully and independently derived by D. J. Bartelink and B. C. DeLoach, Jr.

REFERENCES

1. Prager, H. J., Chang, K. K. N., and Weisbrod, S., "High Power, High Efficiency Silicon Avalanche Diodes at Ultrahigh Frequencies," Proc. IEEE, *55*, No. 4 (April 1967), pp. 586–587.
2. Read, W. T., "A Proposed High-Frequency Negative-Resistance Diode," B.S.T.J., *37*, No. 2 (March 1958), pp. 401–466.
3. DeLoach, Jr., B. C., and Johnston, R. L., "Avalanche Transit-Time Microwave Oscillators and Amplifiers," IEEE Trans. on Electron Devices, *ED-13*, No. 1 (January 1966), pp. 181–186.
4. Scharfetter, D. L., and Gummel, H. K., "Large-Signal Analysis of A Silicon-Read Diode Oscillator," IEEE Trans. on Electron Devices, *ED-16*, No. 1 (January 1969), pp. 64–77.
5. Prager, H. J., Chang, K. K. N., and Weisbrod, S., "Anomalous Silicon Avalanche Diodes for Microwave Generation," Proc. Cornell Conf. on High Frequency Generation and Amplification, August 29–31, Ithaca, N. Y., pp. 266–280.
6. Scharfetter, D. L., Bartelink, D. J., Gummel, H. K., and Johnston, R. L., "Computer Simulation of Low Frequency High Efficiency Oscillation in Germanium" IEEE Solid State Device Research Conference, June 17–19, 1968.
7. Johnston, R. L., and Scharfetter, D. L., "Low Frequency High Efficiency Oscillations in Germanium Impatt Diodes," IEEE Solid State Device Research Conference, June 17–19, 1968; IEEE Trans. El. Dev., *ED-16*, No. 11 (November 1969), pp. 905–911.
8. Johnston, R. L., Scharfetter, D. L., and Bartelink, D. J., "High-Efficiency Oscillations in Ge Avalanche Diodes Below the Transit-Time Frequency," Proc. of IEEE, *56*, No. 9 (September 1968), pp. 1611–1613.
9. Evans, W. J., "Circuits for High Efficiency Avalanche Diode Oscillators," 1969 IEEE G-MTT International Microwave Symposium, May 5–7, 1969, Dallas, Texas, IEEE, *G MTT-17*, No. 12 (December 1969), pp. 1060–1067.
10. Evans, W. J., and Scharfetter, D. L., "Characterization of Avalanche Diode Trapatt Oscillators," IEEE, *GED-17*, No. 5 (May 1970).
11. Bartelink, D. J., and Scharfetter, D. L., "Avalanche Shock Fronts in p-n Junctions," Appl. Phys. Lett., *14*, No. 10 (May 15, 1969), pp. 320–323.
12. DeLoach, Jr., B. C., and Scharfetter, D. L., "Device Physics of Trapatt Oscillators," IEEE Trans. El. Dev., *ED-17*, No. 1 (January 1970), pp. 9–21.
13. Scharfetter, D. L., "High Efficiency Operation of Impatt Diodes," Int. Electron Devices Meeting, October 23–25, 1968, Washington, D. C.

14. Benda, H., and Spenke, E., "Reverse Recovery in Silicon Power Rectifiers," Proc. of IEEE, *55*, No. 8 (August 1967), pp. 1331–1354.
15. Moll, J. L., and Hamilton, S. A., "Physical Modeling of the Step Recovery Diode for Pulse and Harmonics Generation Circuits," Proc. of IEEE, *57*, No. 7 (July 1969), pp. 1250–1259.
16. Dunn, C. N., and Decker, D. R., unpublished work.
17. Ciccolella, D. F., unpublished work.